

Effect of activator on foam properties in sulfurous iron ore flotation

Xiangxiang Chen ^{1,2}, Zhaoyang Zhang ¹, Wen Qiang ¹, Shiyi Huang ¹, Fangzheng Liu ¹, Lu Qiu ¹, Yunfei Ouyang ¹, Tianhao Liu ¹, Shuzhong Liu ¹

¹ Zijin School of Geology and Mining, Fuzhou University, Fuzhou 350108, China

² Fujian Key Laboratory of Green Extraction and High Value Utilization of New Energy Metals, Fuzhou 350108, China

Corresponding author: lsz165157@163.com (Shuzhong Liu)

Abstract: Sulfurous iron minerals with recovery value are contained in a lead-zinc tailing in Fujian Province, China. However, the sulfurous iron minerals are depressed by lime in the early lead-zinc flotation, therefore it is necessary to use appropriate activators to improve the floatability of the mineral. The property of flotation foam can directly reflect the quality of the flotation index. The addition of activators can also change the properties of flotation foam. In this paper, an effective activator combination was selected through actual mine tests and foam analysis. The mineralogical study of the lead-zinc tailing was first carried out through chemical multi-element analysis and XRD. The flotation tests on the recovery of sulfurous iron ore by different activators were carried out. Finally, a foam scanning analyzer was used to test and analyze the frothing performance and froth stability of the slurry under different activation conditions. The results showed that the dispersion-activation flotation and dispersion-combined activation flotation can help to improve the frothing performance of the slurry and improve the flotation indexes. At the same time, the enhanced activated flotation can also reduce the froth stability indexes (FSI) to less than 20 s, and the reduction of the froth stability can help to improve the flotation recovery. For each activation flotation process that achieves the best flotation index, the frothing performance and foam stability of the pulp is close to that of the flotation tests index.

Keywords: pyrite, pyrrhotite, flotation, enhanced activation, froth properties

1. Introduction

Sulfuric acid is an important basic product in the chemical industry, as well as a raw material for many chemical products, and is also used in many other important sectors of the economy (Nleya et al., 2016). The raw materials utilized in the production of sulfuric acid encompass sulfurous iron ore, sulfur (Masotta et al., 2021), and sulfur dioxide-containing flue gases derived from non-ferrous metal pyrometallurgical smelters (Weng et al., 2023). The majority of sulfuric acid is derived from sulfurous iron ore. With the ongoing advancement of the national economy, the demand for raw materials for the manufacture of sulfuric acid is expected to rise.

Sulfurous iron ore is composed of pyrite, pyrrhotite, and albite (Kovalchuk et al., 2024). Given the low content of albite, pyrite, and pyrrhotite are currently the focus of exploitation. Sulfurous iron pyrite is relatively abundant in China, with an estimated reserve of over 4 billion tons. The sulfurous iron pyrite resources are primarily concentrated in the three regions of East China, Central and South China, and Southwest China (Li and Hanaoka, 2020). Despite the abundance of sulfide iron ore resources, the average geological sulfur grade is relatively low, at only 17.68%. Furthermore, there are a greater number of medium and low-grade sulfide iron ore resources, with more than 35% sulphur-rich ore representing only 4% of the total reserves. The floatability of sulfide pyrite is influenced by several factors, including its properties (Jefferson et al., 2023) (e.g., deposit genesis type, crystal system, chemical structure composition, etc.) as well as different pharmaceutical systems, slurry pH (Jiang et al., 2023), and potential (Can et al., 2021). Single pyrite deposits are uncommon, therefore pyrite is frequently found in association with other minerals (Zhang et al., 2022). During the flotation process of sulfide deposits with associated pyrite, pyrite with superior floatability is often hindered from

preferentially separating high-value minerals such as copper, lead, and zinc (Wang et al., 2024). In such instances, inexpensive lime is often employed as an inhibitor of pyrite (Nayak et al., 2022). The recovery of other sulfide ores is also inhibited by the presence of accompanying pyrrhotite. Lime can reduce the oxidation potential of the sulfide iron ore surface (Nyström et al., 2019), resulting in the generation of hydrophilic components such as $\text{Fe}(\text{OH})_3$, CaSO_4 , and $\text{Ca}(\text{OH})_2$ on the sulfide iron ore surface (Bai et al., 2021). This process impairs the flotation of sulfide iron ore after it has been inhibited by lime (John et al., 2020). A considerable number of scholars from both domestic and international academic institutions have conducted a multitude of comprehensive investigations into the activation flotation mechanism of sulfide iron ore and the various factors that influence it.

Nevertheless, most studies currently examining activation mechanisms employ a range of analytical techniques, including zeta potential analysis of mineral surfaces, trap adsorption, Fourier transform infrared spectroscopy (FTIR), XPS, and molecular dynamics simulation. For example, Zhao et al. (2023) demonstrated that SHMP selectively adsorbs on chlorite surfaces and exhibits weak adsorption on specularite surfaces, as evidenced by surface adsorption tests and zeta potential measurements. Gavrilova and Kondrat'ev (2020) implied that physical adsorption effects, as evidenced by the non-geometrical interaction products of activator metals and xanthates, are the probable cause of the activation of sphalerite and pyrite by flotation of zinc ions. This hypothesis explains the observed differences in the activation characteristics of the metals. Zhang et al. (2021) used FTIR to demonstrate that interactions between lead ions and sulfated lapis lazuli surfaces can improve the attachment of xanthates to mineral surfaces. Yang et al. (2023) used X-ray photoelectron spectroscopy (XPS) and time-of-flight secondary ion mass spectrometry (ToF-SIMS) to characterize and found that the Pb species and sulfide products on the surface of chrysocolla increased significantly in the stepwise activation system of Pb^{2+} . The highly active Pb-S fraction on the surface of the chrysocolla was more stable than in the single Pb^{2+} activation system. In the stepwise Pb^{2+} activation system, the Pb species and sulfide products on the surface of chrysocolla increased significantly, the highly active Pb-S fraction on the surface of chrysocolla was higher, and the stability of sulfide products on the surface of chrysocolla was stronger than that in the single Pb^{2+} activation system. Quezada et al. (2021) determined by molecular dynamics simulations that the main interactions for polymer adsorption are through hydroxyl groups on mineral surfaces and COO-Na^+ complexes. Mahrouqi et al. (2017) compared and contrasted the results of zeta potential on natural and artificial calcite and carbonate, and reported new measurements in zeta potential for natural subsurface systems. A foam scanning analyzer can optically determine the frothing performance and froth stability performance of slurry with different activation processes (Fu et al., 2021), to explain the influence of improved activation processes in terms of frothing performance and froth stability performance of slurry to improve the recovery of sulfide iron ore activation. At present, the research on flotation froth performance mainly focuses on frothing agents, but the research on the effect of activators is lacking. For example, Moreno et al. (2021) conducted an evaluation of the dynamic foam stability of 18 nonionic blowing agents from different blowing agent families, employing the degree of foam as a quantitative measure of the ratio of foam height to gas surface velocity. The findings indicated that foaminess exhibited a positive correlation with concentration for all foaming agents tested. Additionally, static foam stability was assessed through the measurement of the half-life and decay rate of foam at varying gas surface velocities and concentrations. Furthermore, there is a paucity of literature examining the characteristics of flotation froth through the use of a foam scanning analyzer. For example, Wang et al. (2018) used a foam scanning analyzer to study the foamability and foam stability of cetyltrimethylammonium bromide (CTAB) solutions with different concentrations. A theory based on foam drainage, bubble coalescence, and coarsening processes was proposed to explain the effect of CTAB concentration on foam performance. Wang et al. (2017) used a foam scanning analyzer to investigate the effects of xanthan gum (XG) and partially hydrolyzed polyacrylamide (HPAM) on the dust suppression foam performance of sodium dodecylbenzene sulfonate (SDBS). This study showed that XG foam has a larger contact area with dust and has a better dust control effect. The highly branched molecular structure of XG and the hydrogen bonds formed play an important role in the dust-related foam performance. Moreover, there is a dearth of literature examining the activation mechanism of sulfide ores.

In this paper, a series of experimental studies were conducted to enhance the activation of a lime-suppressed sulfide iron ore in Fujian Province, China. Subsequently, the impact of different activation techniques on froth flotation performance was evaluated through the use of a foam scanning analyzer. The findings indicated that the enhanced activation flotation pharmaceutical system proposed in this study can enhance flotation indices by modifying both the frothing performance of the slurry and the stability of the froth generated. Consequently, this study offers a valuable contribution to the understanding of flotation activation mechanisms.

2. Materials and methods

2.1. Materials

The ore samples were obtained from the tailings products of a lead-zinc beneficiation plant in Fujian following lead-zinc flotation. To determine the chemical elements with recovery value and their contents in the raw ore, a chemical multi-element analysis was carried out on the tailings, and the results are presented in Table 1. It can be concluded from the analytical results presented in Table 1 that the content of most metallic elements is very low, except for Fe. In contrast, the relative content of S in non-metallic elements is high, indicating that the elements with recovery values are Fe and S, whose relative contents are 25.90% and 8.41%, respectively.

Table 1. Results of chemical multielement analysis of tailings (%)

Element name	P	TFe	S	Mg	Cu	Pb
Relative content	0.069	25.90	8.41	1.97	0.027	0.187
Element name	Al ₂ O ₃	SiO ₂	As	Ca	Zn	
Relative content	6.07	34.45	6.45	6.72	0.208	

Note: The content unit of As is g/Mg

To determine the specific iron- and sulfur-bearing minerals, the main mineral composition of the raw ore was analyzed by XRD, and the results are shown in Fig. 1. As can be seen from Fig. 1, the main iron-containing minerals in the lead-zinc tailings are magnetopyrite, magnetite, and pyrrhotite, and the main sulfur-containing minerals are magneto pyrite and pyrrhotite.

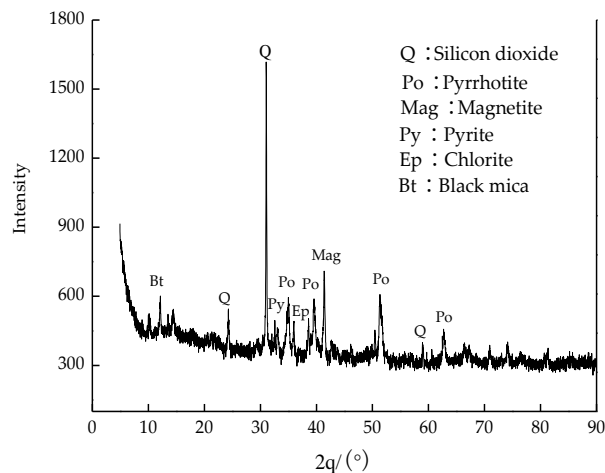


Fig. 1. XRD analysis results of raw ore

For the reagents used in the flotation test, butyl xanthate (C₄H₆OCSSNa, industrial grade, Zhaoyuan Junbang Ore Dressing Reagent Co., Ltd.) and ammonium butylum black ((C₄H₉O)₂PSSNH₄, industrial grade, Zhaoyuan Junbang Ore Dressing Reagent Co., Ltd.) were used as the collectors. Sodium silicate (water glass, Na₂O mSiO₂, industrial grade, Hubei Xinyinhe Chemical Co., Ltd.) and Sodium hexametaphosphate ((NaPO₃)₆, industrial grade, Qingzhou Xincheng Chemical Co., Ltd.) were used as the dispersants. Copper sulfate (CuSO₄, Tianjin BASF Chemical Co., Ltd.), ferrous sulfate (FeSO₄, Tianjin BASF Chemical Co., Ltd.), sodium sulfide (Na₂S, Tianjin Fuchen Chemical Reagent Co., Ltd.),

ammonium bicarbonate (NH_4HCO_3 , Xilong Chemical Industry Co., Ltd.), sulfuric acid (H_2SO_4 , Quanzhou Donghai Reagent Co., Ltd.), oxalic acid ($\text{C}_2\text{H}_2\text{O}_4$, Xilong Chemical Industry Co., Ltd.) of analytically pure were used as the activators.

2.2. Methods

2.2.1. Flotation experiments

In the actual ore flotation test, 500 g of raw ore was weighed each time, and tap water was added to the flotation cell in accordance with the actual situation on site. Solid and liquid flotation chemicals were dissolved in the tap water and prepared into a pre-determined concentration for dosing. The flotation tank of the flotation machine (Xiamen Chenggong Mining Equipment Manufacturing Co., Ltd.) with a capacity of 1.5 dm^3 was used for the roughing and sweeping processes. The selection process was conducted in 1 dm^3 and 0.75 dm^3 flotation tanks. The process flow is illustrated in Fig. 2. To maximize the recovery of sulfur in the sulfur concentrate product, a second process of roughing was employed. The collector is composed of a combination of butyl xanthate and ammonium butylum black, which allows for consideration of both collectability and selectivity.

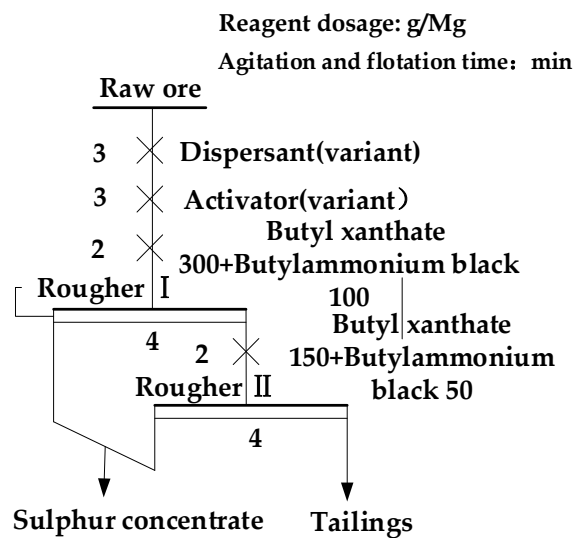


Fig. 2. Flotation process flowsheet

2.2.2. Foam analysis

A foam scanning analyzer (FOAMSCAN, France Teklis Interface Technology Co., LTD) was used for the foam analysis as shown in Fig. 3, which is mainly composed of a foam tube, electric control box, and Foam scanning analysis software. The principle is to inflate the slurry injected into the foam tube by bubbling, the aluminum box has a built-in CCD camera to record the foam phenomenon after the start and subsequent cessation of bubbling, and the Foam scanning and analysis software to analyze the optical changes in the foam tube can be derived from the immediate volume change of the foam; 5 pairs of electrodes installed on the wall of the foam tube can be used for the real-time test of the electrical conductivity of the bubble; 2 electrodes at the bottom of the foam tube can be used for the real-time test of the bubble (Chen et al., 2023). The test method is as follows: To be as close as possible to the actual ore flotation process and facilitate the analysis of the foam scanning analyzer, so in accordance with Fig. 2 roughing once (without scraping bubbles) process for the preparation of the slurry, in accordance with the optimal dosage of each process dosing and mixing, after resting for 10 min to extract the supernatant and placed in the centrifuge for solid-liquid separation, and then extracted from the centrifugal tube in the supernatant foam scanning analyzer related tests and analysis. In the foam scanning analyzer, 70 cm^3 of slurry to be tested was injected with a syringe each time. The parameters were adjusted to set the total test time to 300 s, the bubble time to 100 s, and the inflation volume to $200 \text{ cm}^3/\text{min}$. The instant parameters, such as the foam volume, the volume of slurry in the foam tube, and the foam conductivity, were obtained at the end of the test.

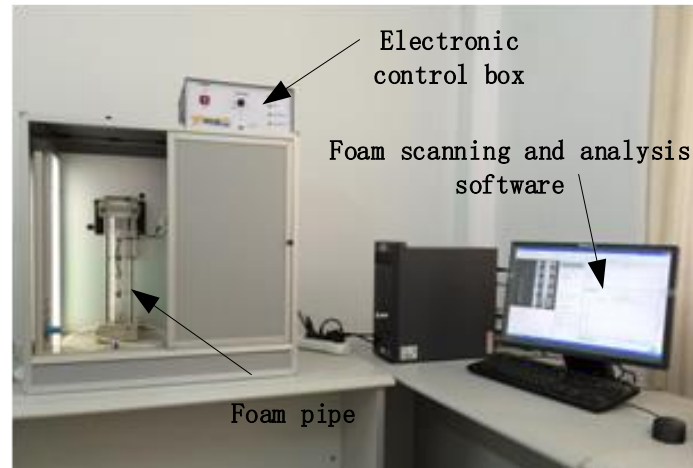


Fig. 3. Foam scanning analyzer

3. Results and discussion

3.1. Flotation experiments

The most effective activators were evaluated based on their respective test indexes. The results are shown in Fig. 4. The conventional activation test revealed that the grade and recovery indexes of the concentrate product were generally lower than those of the other activators. The H_2SO_4 activator exhibited the highest comprehensive index, with a grade and recovery of 32.5% and 43.25%, respectively. In comparison to the unactivated process, in which the sulfur content of the concentrate was 31.41% and the recovery was 11.2%, it can be observed that the sulfurous iron ore suppressed by lime can be more effectively improved in grade and recovery after appropriate activation.

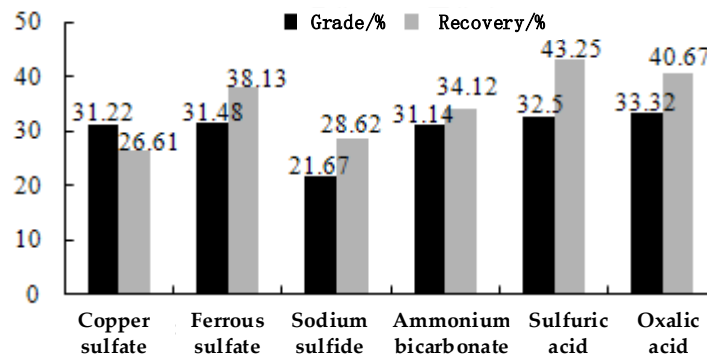


Fig. 4. Comparison results of the best test indexes for conventional activation flotation

In the previous lead-zinc ore dressing operation, the original ore was finely ground, which resulted in the presence of more fine-grained minerals and a high sludge content. The use of dispersants can eliminate the sludge in the target minerals cover phenomenon, thereby activating the strengthening effect (Claremboux, 2020). Consequently, water glass and sodium hexametaphosphate, which are commonly utilized as sludge dispersants, were employed in the flotation test of sulfurous iron ore. This involved first dispersing the ore and then intensifying the activation. In the test, H_2SO_4 , which exhibits optimal performance in conventional activation, was employed as the activator (dose of 1200 g/Mg). Water glass and sodium hexametaphosphate were utilized as the dispersant, respectively, to conduct the flotation process test. The process flow is illustrated in Fig. 2. The influence of the dosage of water glass and sodium hexametaphosphate on the flotation results in the dispersion-enhanced flotation test flow is illustrated in Fig. 5.

It can be seen from the results in Fig. 5(a) that with the increase in the dosage of water glass, the recovery of sulfur in the concentrate showed a slow decline, and the grade also began to decline slowly after the dosage of 400 g/Mg of water glass, which can be determined to be the optimal dosage of

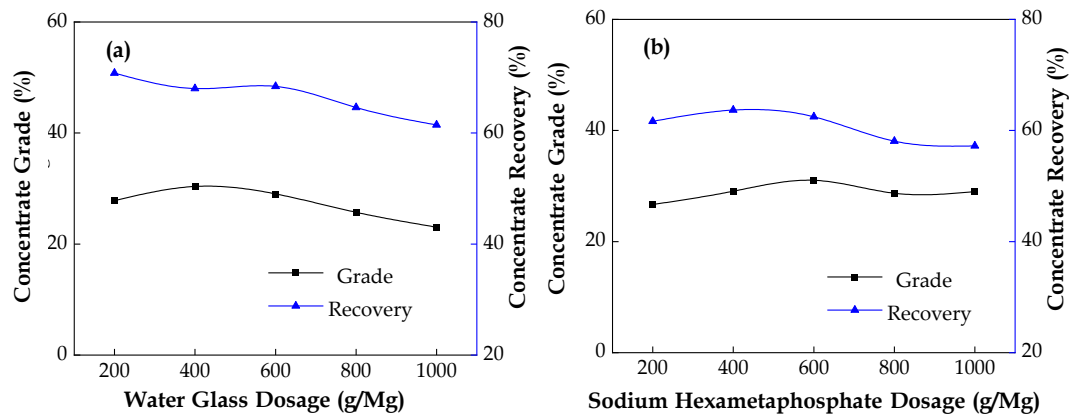


Fig. 5. Effect of sodium hexametaphosphate dosage on flotation results (a); effect of water glass dosage on flotation results (b)

400 g/Mg of water glass, and at this time the sulfur grade and the recovery can reach 30.38% and 68.02%, respectively. In terms of recovery rate, water glass has a dispersing effect on the slime, but it will also cause some target minerals to absorb water glass on their surface, affecting their floating, so the recovery rate is inversely proportional to the amount of water glass added. In terms of grade, water glass also has a certain inhibitory effect on quartz and silicate gangue minerals in the original ore, so adding a proper amount of water glass can improve the grade, but adding too much water glass will increase the viscosity of the solution and cause the grade to decrease. From the test results in Fig. 5(b), it can be seen that the recovery of sulfur in the concentrate reaches the maximum value of 63.69% when the dosage of sodium hexametaphosphate is 400 g/Mg, and the grade can reach a high 29.05%, so the optimal dosage of sodium hexametaphosphate is determined to be 400 g/Mg. Compared with the effect of the conventional activation flotation process, the dispersion-activation flotation process can greatly improve the recovery of sulfur in the concentrate with a slight decrease in the grade. A comprehensive comparison was conducted to determine the optimal test index for water glass. The results demonstrated that water glass, in addition to the sludge, has a dispersing effect. The presence of quartz and silicate vein minerals in the original ore also exhibited an inhibitory effect, which enhanced the subsequent activator's effect on the surface of sulfurous iron ore (Deng et al., 2019). Subsequently, a dispersion-activation flotation pilot study was conducted at a water glass dosage of 400 g/Mg, with dispersion followed by conventional activation. The process flow is illustrated in Fig. 2.

The initial dispersion is followed by the addition of a variety of single activators, which serve as the best indicators for each flotation process. The results are presented in Fig. 6. Fig. 6 illustrates that dispersion enhances the flotation test process, identifying the optimal combination of chemicals for the water glass and $C_2H_2O_4$. The system agent grade and recovery are 29.2% and 73.62%, respectively. In comparison to the H_2SO_4 activator (grade and recovery of 32.5% and 43.25%, respectively), which exhibits the optimal comprehensive index of conventional activation flotation, the recovery has been markedly enhanced despite a slight decline in grade. The enhanced activation effect is evident. Moreover, the recoveries of sulfur concentrates in dispersion-activation flotation were all significantly enhanced in comparison to those observed in conventional activation flotation, although the grades were mostly slightly decreased. This may be due to the first dispersed and then activated flotation process to strengthen the effect of activation recovery (Zhou et al., 2020), while in the previous lead-zinc beneficiation after the grinding of raw ore and slime particle size will be finer, in the process of froth flotation of the raw ore may be entrained with part of the fine-grained chalcopyrite minerals, and thus in the recovery of increased at the same time, grade due to the increase in the entrainment of chalcopyrite minerals and a decline in the grade (Taner et al., 2024).

After determining that water glass is the optimal dispersant for dispersion-activation flotation, the experimental study of a single activator yielded more favorable results. A synergistic effect may exist between the activators (Wang et al., 2022), which may explain the improved index observed. Consequently, several activators with superior indexes in the dispersion-activation flotation test were subjected to the experimental study of dispersion and combined activation flotation. Four combinations

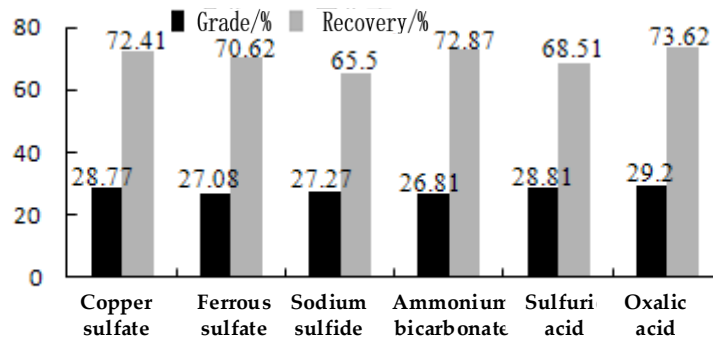


Fig. 6. Comparison results of the best indicators of dispersion-activation flotation

of activating agents (Combination 1: $C_2H_2O_4 + FeSO_4$; Combination 2: $C_2H_2O_4 + NH_4HCO_3$; Combination 3: $H_2SO_4 + CuSO_4$; Combination 4: $FeSO_4 + NH_4HCO_3$) were selected for the study.

Dispersion-combined activation flotation test method: When the dosage of dispersant water glass is 400 g/Mg, first determine the optimal ratio of the activation agent combination under the premise of fixing its total dosage, and then determine the optimal indicators achieved by the activation agent combination at its optimal dosage under this ratio. The process flow is shown in Fig. 2. The best sulfur concentrate indexes of the above four enhanced flotation test flows of dispersing first and then using activator combinations (Combination 1: $C_2H_2O_4 + FeSO_4$; Combination 2: $C_2H_2O_4 + NH_4HCO_3$; Combination 3: $H_2SO_4 + CuSO_4$; and Combination 4: $FeSO_4 + NH_4HCO_3$) are compared by this summary, and the comparison results are shown in Fig. 7. As can be seen from Fig. 7, in the dispersion-combined activation flotation test, the positive synergistic effect of the combination of agents is combination 1 ($C_2H_2O_4 + FeSO_4$) and combination 2 ($C_2H_2O_4 + NH_4HCO_3$), both of which have improved flotation recovery compared to the original dispersed enhancement after dispersion-combined activation enhancement. On the other hand, the flotation effect of combination 3 ($H_2SO_4 + CuSO_4$) and combination 4 ($FeSO_4 + NH_4HCO_3$) activation was the opposite, producing a negative synergistic effect. The grade and recovery of sulfur in the concentrate obtained by the combination of water-glass dispersion and then $C_2H_2O_4 + FeSO_4$ activation enhanced flotation can reach 27.3% and 77.45%, respectively, while the grade and recovery achieved by water-glass dispersion and then $C_2H_2O_4$ activation flotation are 29.2% and 73.62%, respectively, and that of water-glass dispersion and then $FeSO_4$ activation flotation are 27.08% and 70.62%, respectively. and 70.62% respectively. It can be shown that the combination of water glass dispersion and $C_2H_2O_4 + FeSO_4$ activation-enhanced flotation has a better recovery effect. In addition, the combination of water glass dispersion followed by $C_2H_2O_4 + NH_4HCO_3$ activation enhanced flotation could obtain sulfur concentrates with sulfur grade and recovery of 28.86% and 73.82%, respectively. Compared with the effect of first water glass dispersion and then $C_2H_2O_4$ activated flotation, the grade of sulfur in the concentrate decreased slightly and the recovery increased slightly, while compared with the grade and recovery achieved by first water glass dispersion and then

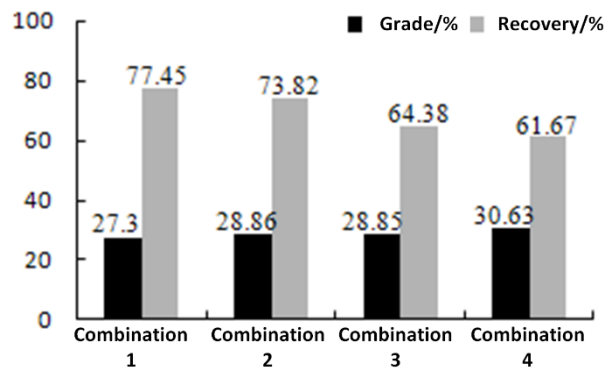


Fig. 7. Comparison results of the best indicators of dispersion-combined activation flotation. Combination 1: $C_2H_2O_4 + FeSO_4$; Combination 2: $C_2H_2O_4 + NH_4HCO_3$; Combination 3: $H_2SO_4 + CuSO_4$; Combination 4: $FeSO_4 + NH_4HCO_3$

NH_4HCO_3 activated flotation (26.81%, 72.87%, respectively), the grade and recovery were both improved. It can be shown that some dispersion-combined activation flotation has a better-enhanced activation recovery effect than dispersion-activation flotation in terms of improving recovery, especially the combination 1 $\text{C}_2\text{H}_2\text{O}_4 + \text{FeSO}_4$ can reach the highest recovery of 77.45%. For Combination 1, the activation mechanism of $\text{C}_2\text{H}_2\text{O}_4$ is the same as that of sulfuric acid. It can clean the oxide film on the surface of pyrite and expose a fresh surface. It can also increase the redox potential of the pyrite surface and prevent it from further oxidation. In addition, $\text{C}_2\text{H}_2\text{O}_4$ as an activator is not as corrosive to equipment as sulfuric acid, which is conducive to its promotion and application. FeSO_4 is used as an activator because it will hydrolyze into Fe^{2+} and SO_4^{2-} when added to the solution. The presence of both can increase the oxidation potential of the pyrite surface and prevent further oxidation of the pyrite.

3.2. Foam properties

The frothing properties of the slurry and the stability of the generated froth can both influence the flotation behavior of minerals (Liu et al., 2020). The foam scanning analyzer can be utilized to ascertain the frothing performance and froth stability of the slurry in unactivated flotation, conventional activation flotation, dispersion-activation flotation, and dispersion-combined activation flotation. Additionally, it can be employed to determine the impact of dispersion-activation and dispersion-combined activation flotation in enhanced flotation on the improvement of flotation indexes in terms of the two performances. The foam scanning analyzer is capable of measuring the instantaneous values of froth volume, froth conductivity, and slurry volume in the frothing tube, while also utilizing the coefficient of froth expansion (Froth Expansion or FE), which is defined as the ratio of the froth volume at the time of stopping the bubbling to the volume of the slurry reduced by the process (see Eq. 1), the foam capacity coefficient (Froth Capacity or FC), which is defined as the ratio of the foam volume to the inflated volume in the foam tube when stopping foaming (as shown in Eq. 2), is used to characterize the foaming performance. The slurry can be analyzed by taking the value of the curves formed by the instantaneous change in conductivity in the foam and then calculating the FSI to characterize the foam stability according to Eq. 3. The FSI is calculated according to Eq. 3 to characterize the foam stability. The equations are presented below, and the parameter identification in each formula is shown in Fig. 8:

$$\text{FE} = \frac{V_{\text{froth}}}{V_{\text{liq}} - V_{\text{liq}}} \quad (1)$$

$$\text{FC} = \frac{V_{\text{froth}}}{V_{\text{gas}}} \quad (2)$$

$$\text{FSI} = C_0 \cdot \frac{\Delta t}{\Delta C t} \quad (3)$$

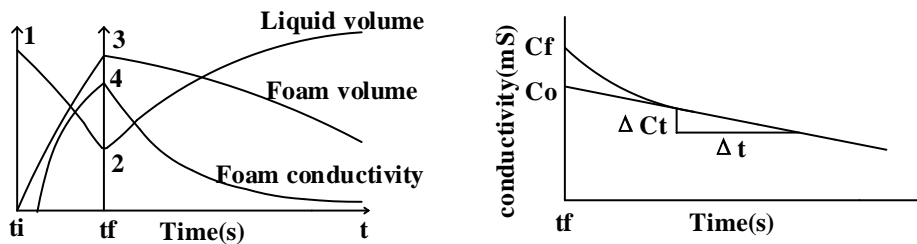


Fig. 8. Identification of the parameters of each formula. t_i : Start foaming time; t_f : Stop foaming time; 1 : Initial liquid volume (V_{liq}); 2 : Volume of liquid that stops bubbling (V_{liq}); 3 : Stop bubble volume (V_{froth}); 4 : Stop bubble foam conductivity (C_f); Δt : Foam conductivity curve phase time difference; $\Delta C t$: Foam conductance difference corresponding to phase time difference; C_0 : The corresponding foam conductance at the slope of $\Delta C t / \Delta t$

The slurry produced by one roughing of the unactivated flotation test (dosage of chemicals: butyl xanthate 300 g/Mg + ammonium butylum black 100 g/Mg) was subjected to analysis by the foam scanning analyzer. Figure 9(a) depicts the instantaneous volume of froth that can be measured, while Fig. 9(b) illustrates the instantaneous values of the liquid volume in the froth tube and the froth

conductivity. From Fig. 9(a), it can be observed that the volume of the foam produced by unactivated flotation rapidly expanded and reached a high level during the initial stage of bubbling, from 0 s to 100 s. The foam volume reached a maximum of 21.98 cm³ during the bubbling process and subsequently decreased to reach a volume of 17 cm³ by the end of the bubbling period at 100 s. The volume of the foam continued to fluctuate throughout the bubbling process, reaching a maximum of 25 cm³. This indicated that the liquid was capable of foaming. However, upon cessation of the bubbling, the foam volume rapidly decreased to a lower level, approaching zero. This suggests that the generated foam was unstable. As illustrated in Fig. 9(b), the conversion of liquid volume into foam volume was observed to commence at the onset of bubbling. This conversion results in a rapid decrease in liquid volume, reaching a certain value. Thereafter, a stabilization phase ensues, during which no further decrease in liquid volume is observed. Upon cessation of bubbling after 100 s, a rapid increase in liquid volume is observed, approaching its initial value. The time required for the foam volume to decrease to 0 cm³ after the bubbling stops in Fig. 9(a) is essentially the same as the time required for the liquid volume to reach its initial value. However, the final liquid volume will not be equal to its initial value due to the small amount of liquid volume adhering to the foam tube wall throughout the test phase. This is due to the continuous expansion and rupture of the foam. This is because a small amount of the liquid volume will adhere to the walls of the foam tube throughout the test phase due to the continuous expansion and rupture of the foam. Furthermore, during the bubbling phase, which lasts from 0 to 100 seconds, as the foam volume increases, the liquid content between the pairs of detection electrodes on the foam tube wall begins to increase. This is accompanied by a gradual rise in the detected conductance, which reaches its highest value near the end of the bubbling phase. The value is observed near the conclusion of the bubbling phase. After the conclusion of the bubbling phase, as the foam volume declines at a rapid pace, the liquid content between the pairs of detection electrodes on the foam tube wall declines, and the conductance of the foam decreases rapidly to the initial value.

The specific parameters of the unactivated flotation and the FE, FC, and FSI calculated according to the formulae are presented in Table 2. As illustrated in Table 2, when the end point of 100 s bubbling is reached, with a total injected gas volume of 330 cm³, it can be determined that the liquid volume consumed is 5.69 cm³ (69.05 cm³ - 63.36 cm³) can produce 17.25 cm³ of froth; and then by the above formula, it can be obtained that FE=3.03, FC=0.05, FSI = 20 s in the unactivated flotation process.

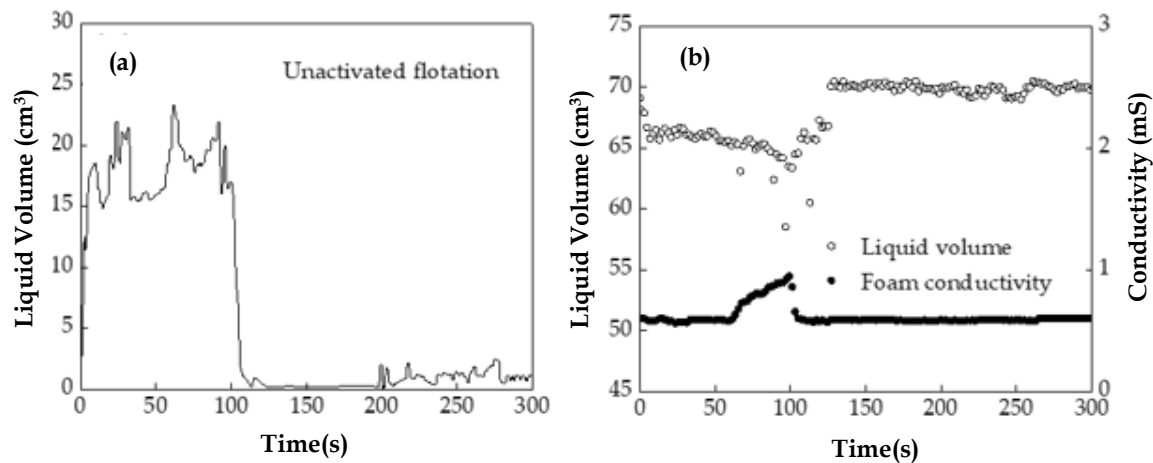


Fig. 9. Effect of unactivated flotation on foam volume (a); effect of unactivated flotation on liquid volume and foam conductance in the foam tube (b)

Table 2. Unactivated flotation foam scanning analyzer parameters

Parameters	Initial liquid Volume (cm ³)	Final Foam Volume (cm ³)	Final Liquid Volume (cm ³)	Injected Gas Volume (cm ³)	FE	FC	FSI (s)
Unactivated process	69.05	17.25	63.36	330	3.03	0.05	20

The slurry generated from one roughing of each optimal flotation test process of conventional activation (the dosage of trapping agent is 300 g/Mg of butyl xanthate + 100 g/Mg of ammonium butylum black; the dosage of activator is 250 g/Mg of CuSO_4 , 200 g/Mg of FeSO_4 , 400 g/Mg of Na_2S , 300 g/Mg of NH_4HCO_3 , 1200 g/Mg of H_2SO_4 , and 1200 g/Mg of $\text{C}_2\text{H}_2\text{O}_4$) was analyzed. The comparison of the instant volume of foam obtained from the test is shown in Fig. 10. As seen in Fig. 10, the conventional activation flotation test process begins with the formation of bubbles, which rapidly expand to a higher volume. As this occurs, the fluctuations in foam volume become smaller, although they are not as pronounced as those observed in the unactivated flotation process. The conventional CuSO_4 and $\text{C}_2\text{H}_2\text{O}_4$ activation in the bubble process results in greater foam fluctuations than other conventional activation flotation processes. This may indicate that the two processes have poorer slurry foaming performance. The conventional activation flotation process resulted in a higher peak foam volume than the unactivated flotation process. This indicates that the use of conventional activation flotation is conducive to increasing the frothing performance of flotation slurry. In comparison to the other activation processes, the conventional FeSO_4 activation process exhibited a faster decline in foam volume after reaching a peak, indicating that its foam stability is the least stable among the conventional activation flotation processes.

To illustrate further, the effects of conventional activation flotation processes on liquid volume in the froth tube and conductivity of generated froth were analyzed in conjunction with conventional activation flotation processes in Fig. 11 and calculated by the formula. As illustrated in Fig. 11, the effect of different activators on the liquid volume in the froth tube of conventional activation flotation

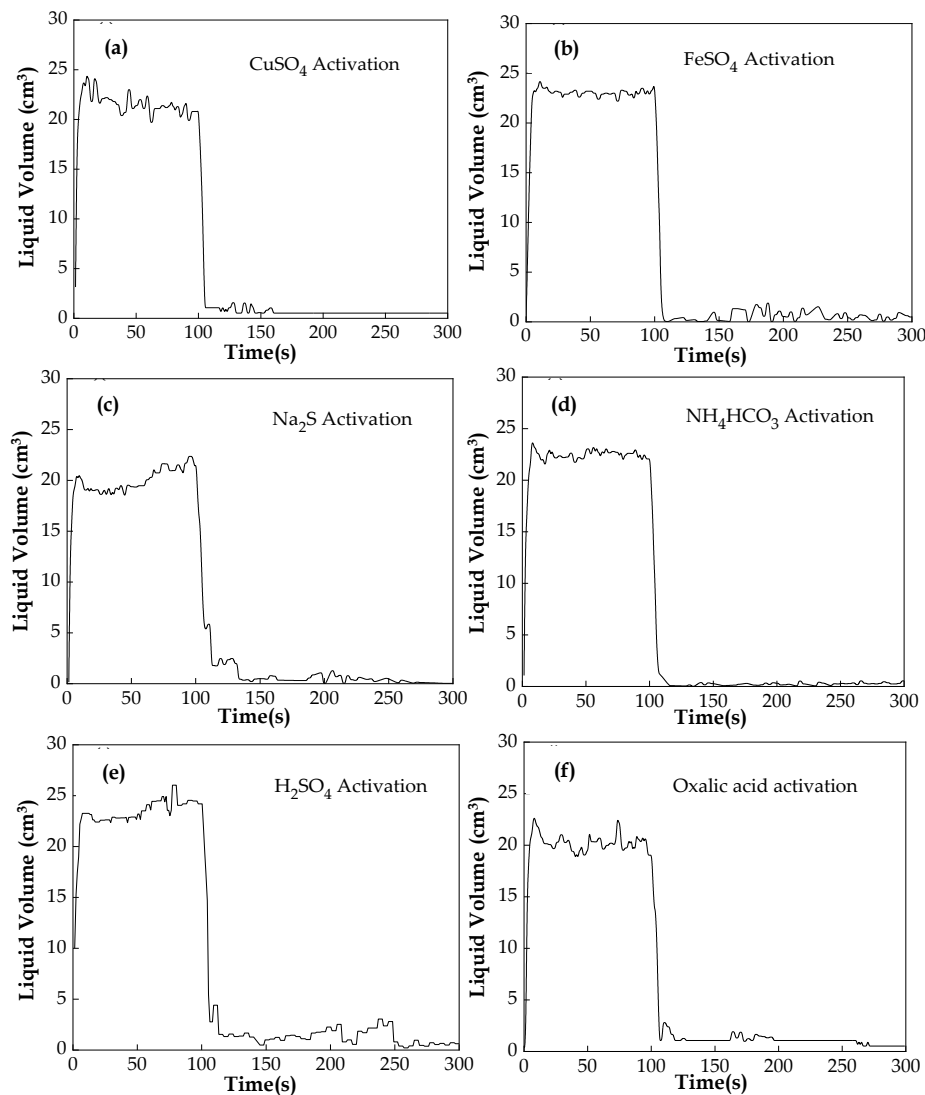


Fig. 10. Effect of conventional activation on froth volume

demonstrates that to generate the froth volume of Fig. 10. Each activation process consumes approximately 5 cm³ of liquid volume, with all of them occurring at the beginning of the bubble stage. Thereafter, the liquid volume decreases rapidly, reaching a certain stable value with minor fluctuations. Following the end of the bubble, the liquid volume rises rapidly to a value close to the initial value. The addition of activators in conventional activation flotation can increase the conductivity of the foam. This is because the activator belongs to inorganic salts, inorganic acids, and organic acids. This is equivalent to increasing the electrolyte content in the slurry, and thus increasing the electrolyte content in the generated foam. Consequently, the conductivity of the generated foam is also increased. Due to the diverse types and quantities of activators employed, the conductivity of the foam generated by each process cannot be directly compared.

The specific parameters of conventional activation flotation and the FE, FC, and FSI can be calculated according to the formulas by substituting the values obtained from Figures 10 and 11 into the formulas. The results are presented in Table 3. As seen in Table 3, the FE value of conventional CuSO₄ and C₂H₂O₄ activation is smaller, indicating that the foam undergoes greater fluctuations during the bubbling process than in other conventional activation flotation processes. The FSI value of 15 s in conventional FeSO₄ activation is the lowest, so its foam stability is the worst in conventional activation flotation, which corresponds to the results in Fig. 10. In comparison to the unactivated flotation (FE=3.03, FC=0.05, FSI=20 s), all the FE, FC, and FSI (except for H₂SO₄) obtained by parameter calculations in the conven-

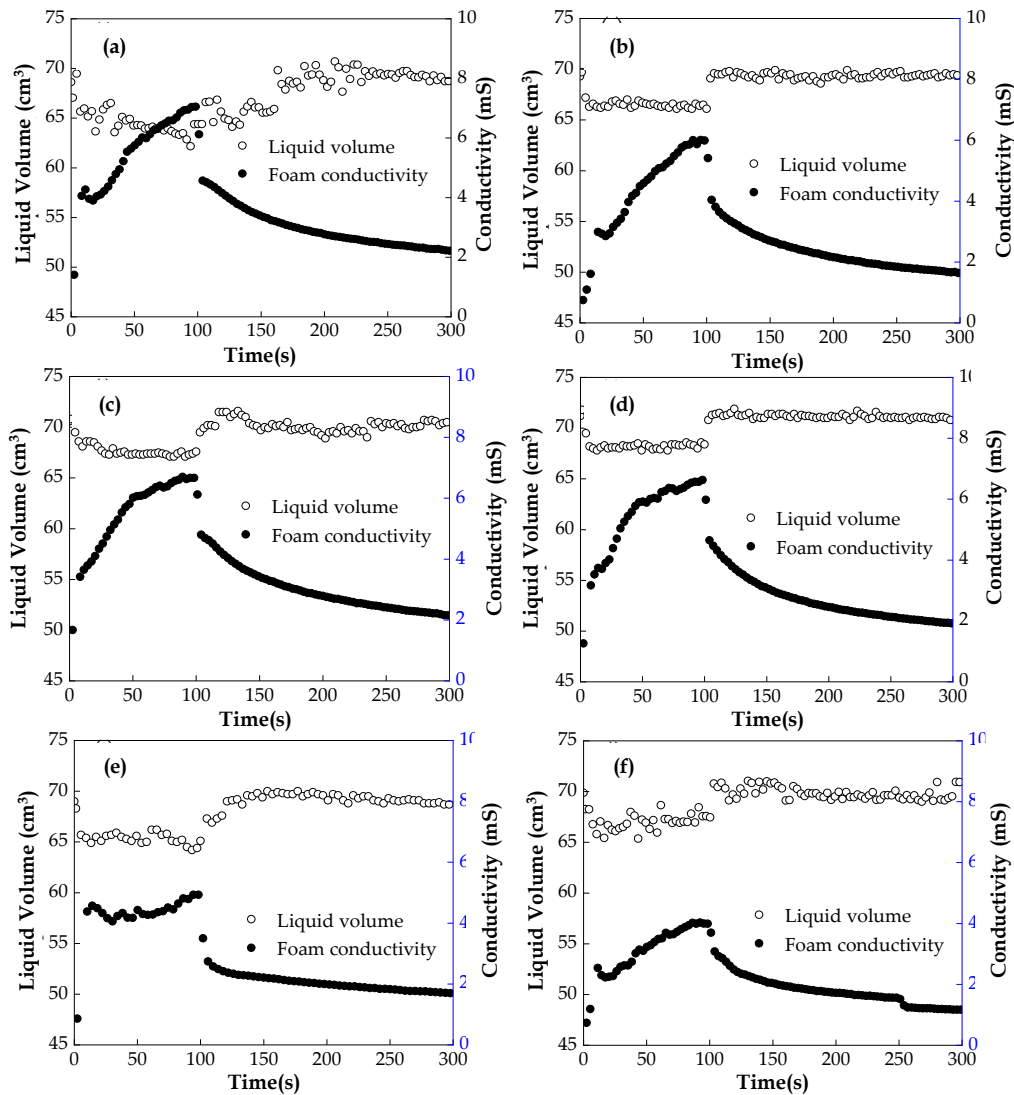


Fig. 11. Effect of conventional activation on the volume of liquid in the froth tube and the conductance of the generated foam. (a) CuSO₄ activation (b) FeSO₄ activation (c) Na₂S activation (d) NH₄HCO₃ activation (e) H₂SO₄ activation (f) C₂H₂O₄ activation

tional activation flotation exhibited an improvement in comparison to the unactivated flotation. The froth parameters, including the FE, FC, and FSI, also indicated that the increase in foam parameters, including the FE, FC, and FSI, also indicates that the foam The performance and stability of the generated foam in the conventional activation flotation process are superior to those observed in the unactivated process. Consequently, the final flotation results are also affected, with the sulfur recovery of the concentrate being enhanced in the conventional activation flotation process compared to the unactivated flotation process. The optimal flotation index in the conventional activation flotation process is observed in the H₂SO₄ activated process, with an FE of 7.36, FC of 0.07, and FSI of 21 s.

Table 3. Foam scanning analyzer parameters of conventional activation flotation

Parameters	Initial Liquid Volume (cm ³)	Final Foam Volume (cm ³)	Final Liquid Volume (cm ³)	Injected Gas Volume (cm ³)	FE	FC	FSI (s)
CuSO ₄	69.10	24.20	64.40	332	5.15	0.07	32
FeSO ₄	71.21	22.07	68.42	332	7.91	0.07	15
Na ₂ S	71.01	20.70	67.56	332	6.00	0.06	26
NH ₄ HCO ₃	69.88	21.23	67.46	332	8.77	0.06	30
H ₂ SO ₄	69.35	23.78	66.12	332	7.36	0.07	21
C ₂ H ₂ O ₄	68.63	19.03	64.40	332	4.50	0.06	23

The sample preparation conditions for the dispersion-activation flotation process were as follows: the dosage of the trapping agent was butyl xanthate (300 g/Mg) and ammonium butylum black (100 g/Mg), the dosage of the dispersant was water glass (400 g/Mg), and the dosage of the activator was CuSO₄. The concentrations of the reagents were as follows: 200 g/Mg FeSO₄, 250 g/Mg Na₂S, 400 g/Mg NH₄HCO₃, 600 g/Mg H₂SO₄, and 1600 g/Mg C₂H₂O₄, respectively. The comparison of the instantaneous volume of foam obtained from the test is shown in Fig. 12. As illustrated in Fig. 12, the dispersion-activation flotation process is characterized by a rapid expansion of foam volume at the onset of the bubble, followed by a period of relatively stable fluctuations. These fluctuations are less pronounced than those observed in the unactivated flotation process, which is attributed to the dispersion and subsequent activation of sulfuric acid. The activation process in the dispersion-activation flotation process results in greater fluctuations in the bubble volume than in the conventional activation process. Consequently, the slurry foaming performance may be poorer. Furthermore, the majority of the foam volume in the dispersion-enhanced flotation process is higher than in the other dispersion-activation flotation processes. In contrast to the conventional activation process, the majority of the foam volume in dispersion-activation flotation (e.g., CuSO₄, FeSO₄, NH₄HCO₃ activation) rapidly diminishes to nearly 0 cm³ following the cessation of the bubbling process. This observation suggests that the foam stability of dispersion-activation flotation is suboptimal.

As illustrated in Fig. 13, the dispersion-activation flotation process results in a reduction in the volume of liquid in the froth tube. To achieve the froth volume depicted in Fig. 12, each activation process requires a volume of liquid of approximately 5 cm³, which initially decreases rapidly, then remains stable, and finally rises rapidly to a value close to the initial value when the froth is finished. Moreover, the effect of dispersion-activation flotation on froth conductivity, as illustrated in Fig. 13, reveals that, in a manner analogous to the activation process previously described, the addition of the electrolyte activator resulted in an increase in electrolyte concentration within the slurry, consequently enhancing the conductivity of the generated froth relative to the unactivated flotation process. From the values obtained in Figures 12 and 13, and by substituting the three formulas previously mentioned, calculations can be made to obtain the specific parameters of the dispersion-activation flotation process and the FE, FC, and FSI, which are calculated according to the formulas. The results are presented in Table 4. As illustrated in Table 4, the FE of the initial dispersion and subsequent H₂SO₄ activation process represents the lowest value observed in the dispersion-activation flotation process, indicating a suboptimal slurry foaming performance. In comparison to the conventional activation process, the dispersion-activation flotation FSI exhibits diminished foam stability. Furthermore, when benchmarked

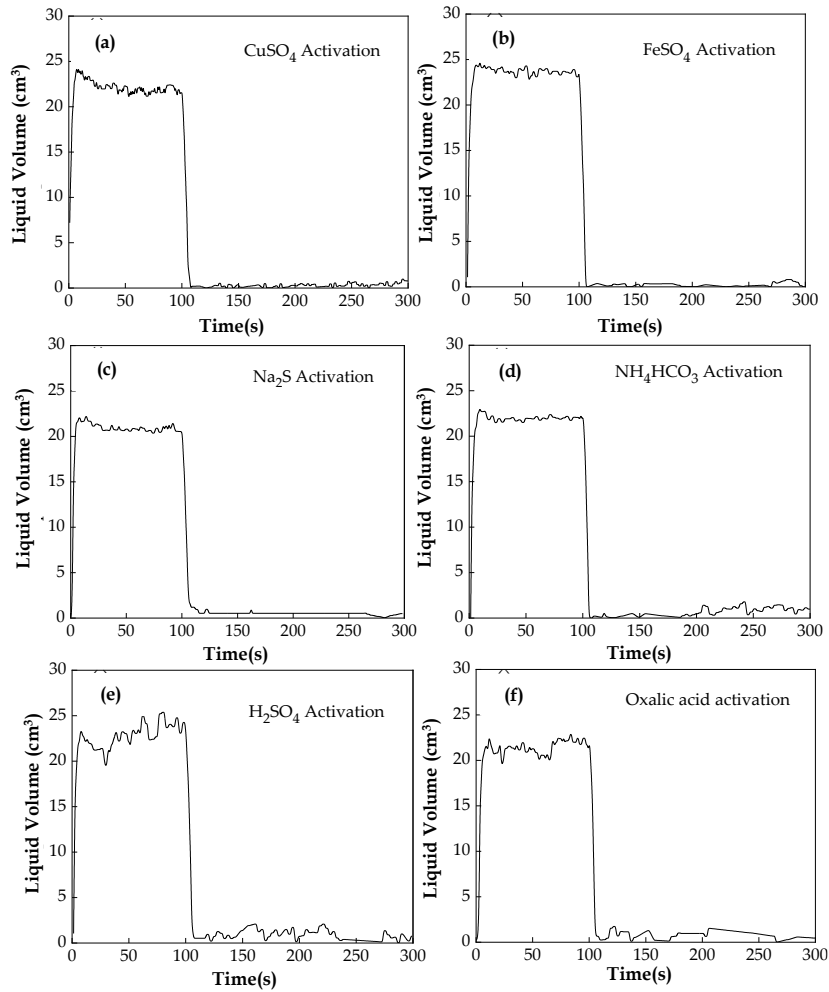


Fig. 12. Effect of dispersion-activation flotation on froth volume

against the unactivated flotation process (FE=3.03, FC=0.05), the dispersion-activation flotation process is observed to exhibit inferior performance. The dispersion-activation flotation process is obtained by parameter calculations of the entire FE, FC, and FSI, which are improved compared to the unactivated flotation process. However, the FSI is partially decreased. In contrast, the conventional activation flotation process yields the best H₂SO₄-activated flotation process (FE=7.36, FC=0.07, FSI=21 s) in terms of the actual flotation index.), dispersed strengthened flotation process in the actual flotation index of the best C₂H₂O₄-activated flotation process (FE=7.53, FC=0.07, FSI=15 s), dispersed strengthened flotation process in the actual flotation index of the best C₂H₂O₄-activated flotation process (FE=7.53, FC=0.05, FSI=15 s). In this case, the FE and FC, which are used to characterize the foaming performance of the slurry, are both very close, while the FSI varies greatly.

Table 4. Foam scanning analyzer parameters of dispersion-activation flotation

Parameters	Initial Liquid Volume (cm ³)	Final Foam Volume (cm ³)	Final Liquid Volume (cm ³)	Injected Gas Volume (cm ³)	FE	FC	FSI (s)
CuSO ₄	71.93	21.54	69.30	332	8.21	0.06	17
FeSO ₄	68.85	23.74	65.13	332	6.39	0.07	18
Na ₂ S	68.67	20.54	65.38	332	6.24	0.06	21
NH ₄ HCO ₃	67.99	22.21	64.25	332	5.94	0.07	13
H ₂ SO ₄	67.90	24.26	63.70	332	5.78	0.07	20
C ₂ H ₂ O ₄	68.51	22.03	65.58	332	7.53	0.07	15

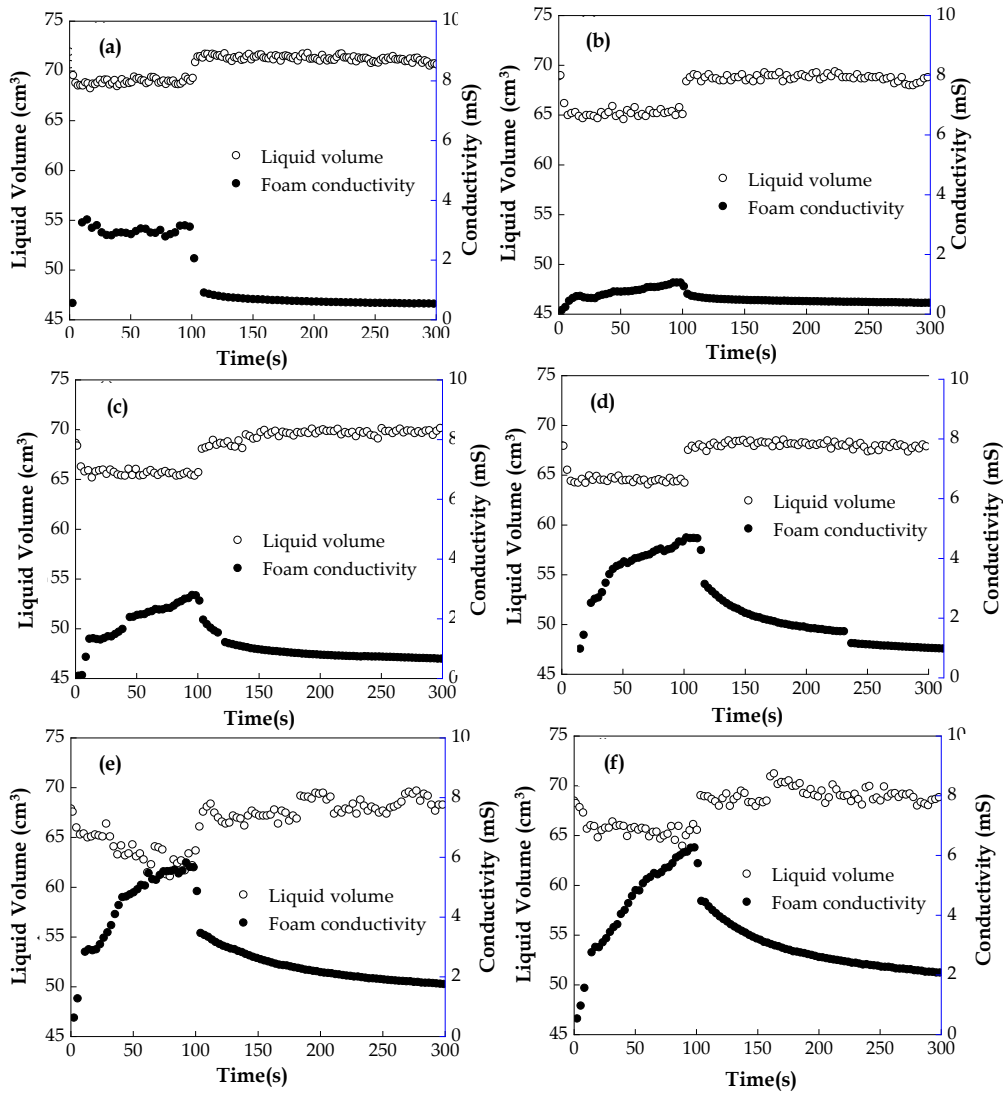


Fig. 13. Effect of dispersion-activation on the volume of liquid in the froth tube and the conductivity of the generated foam. (a) CuSO_4 activation, (b) FeSO_4 activation, (c) Na_2S activation, (d) NH_4HCO_3 activation, (e) H_2SO_4 activation, (f) $\text{C}_2\text{H}_2\text{O}_4$ activation

The pulp produced by the primary roughing of each optimal flotation test process with conventional activation (the collector dosage is 300 g/Mg of butyl xanthate + 100 g/Mg of ammonium butylum black powder; the activator dosages are CuSO_4 250 g/Mg, FeSO_4 200 g/Mg, Na_2S 400 g/Mg, NH_4HCO_3 300 g/Mg, H_2SO_4 1200 g/Mg, $\text{C}_2\text{H}_2\text{O}_4$ 1200 g/Mg, respectively) was analyzed by foam scanning analyzer. The comparison of the instant foam volume obtained in the test is shown in Fig. 14. From Fig. 14, it can be seen that in the dispersion-combined activation flotation process, with the beginning of the bubble, as in the dispersion-activation flotation process and the conventional activation flotation process, the foam volume rapidly expands to a higher value, and there will be a small fluctuation when it reaches the peak value; the peak value of the foam of the dispersion-combined activation flotation process is higher than that of the unactivated flotation process, and it is close to that of the dispersion-activation flotation and the conventional activation flotation; dispersed $\text{C}_2\text{H}_2\text{O}_4 + \text{NH}_4\text{HCO}_3$ combination activation in the bubbling process foam fluctuation is greater than other combinations, so its slurry foaming performance is poor.

As can be seen from the effect of the dispersion-combined activation flotation process on the volume of liquid in the froth tube in Fig. 15, the generation of the froth volume in Fig. 14, like the two flotation processes described above, consumes about 5 cm^3 of liquid volume for each activation process, and all of them have a rapid decrease in the volume of liquid at the beginning of the froth stage, which is then

maintained at a stable level, and then the volume of liquid rapidly increases to close to the initial value at the end of the froth. In addition, from the effect of dispersion-combined activation flotation on the liquid volume in the froth tube and the froth-generating conductivity in Fig. 15, it can be seen that, as with the two activation processes described above, the addition of the electrolyte activator increased the electrolyte in the slurry and thus also increased the froth-generating conductivity relative to the unactivated flotation process. To further compare the differences in frothing performance and foam stability of the slurry between different dispersion-combined activation flotation processes, the specific parameters of the dispersion-combined activation flotation process and the FE, FC, and FSI calculated based on the formulas can be obtained from the values obtained from Figs. 14 and 15 and then substituted into the three equations mentioned above. The results are given in Table 5.

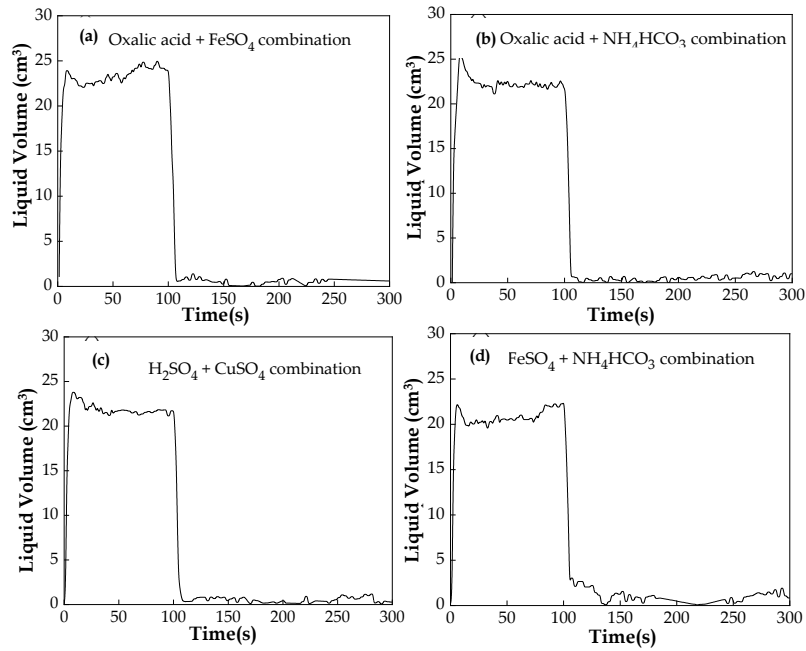


Fig. 14. Effect of dispersion-combined activation on froth volume

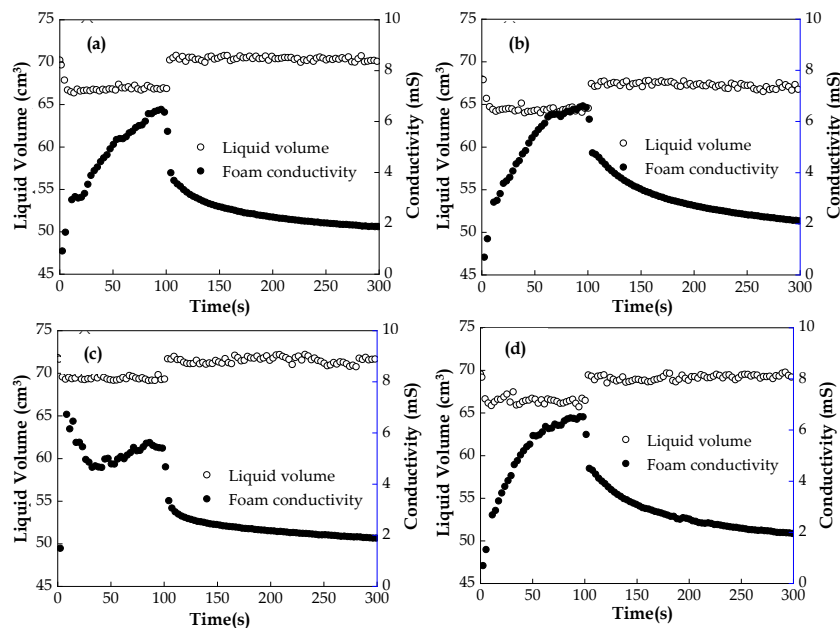


Fig. 15. Effect of dispersion-combined activation flotation on the volume of liquid in the froth tube and the conductivity of the generated foam. The following combinations were evaluated: (a) $C_2H_2O_4 + FeSO_4$, (b) $C_2H_2O_4 + NH_4HCO_3$, (c) $H_2SO_4 + CuSO_4$, and (d) $FeSO_4 + NH_4HCO_3$

Table 5. Foam scanning analyzer parameters of dispersion-combined activation flotation

Parameters	Initial Liquid	Final Foam	Final Liquid	Injected Gas	FE	FC	FSI (s)
	Volume (cm ³)						
C ₂ H ₂ O ₄ +FeSO ₄	70.25	23.97	66.89	332	7.13	0.07	18
C ₂ H ₂ O ₄ +NH ₄ HCO ₃	67.99	21.74	64.56	332	6.33	0.07	14
H ₂ SO ₄ +CuSO ₄	71.83	21.73	69.33	332	8.67	0.07	12
FeSO ₄ +NH ₄ HCO ₃	69.57	22.45	66.47	332	7.25	0.07	15

As can be seen from Table 5, the FE value of dispersed and then C₂H₂O₄ + NH₄HCO₃ combination activation is the smallest, 6.33, so its slurry foaming performance is poor; all the dispersion-combined activation flotation process FSI < 20 s, its foam stability is poor; compared with the unactivated flotation process (FE = 3.03, FC = 0.05, FSI = 20 s), dispersion-combined activation flotation process through the parameter calculation to get all the FE, FC, are higher than the unactivated flotation process, while all the FSI is lower than the unactivated flotation process; compared with the conventional activation flotation process in the actual flotation index of the best H₂SO₄ activation (FE = 7.36, FC = 0.07, FSI = 21 s), dispersion-combined activation to strengthen the flotation process of the actual flotation index of the best for the C₂H₂O₄ + FeSO₄ activation process (FE=7.13, FC=0.07, FSI=18 s), in which the FE and FC, which characterize the frothing performance of the slurry, are very close to each other, while the FSI has decreased; compared with the dispersion enhanced flotation process (the best actual flotation index is the C₂H₂O₄ activation process: FE=7.53, FC=0.07, FSI=15 s), in which FE and FC are very close to each other, while there is a difference in FSI.

The analysis results of the foam scanning analyzer in different activation flotation processes were combined with the actual ore flotation indexes as presented in Table 6. The comparison results revealed that the FE values of the unactivated flotation process are considerably smaller than those of the other flotation processes. This indicates that the activated flotation process facilitates enhanced foaming

Table 6. Comparative results of flotation index and foam scanning analyzer parameters for different activation processes

Activation Process	Grade (%)	Recovery (%)	FE	FC	FSI (s)
Unactivated	31.41	11.20	3.03	0.05	20
CuSO ₄	31.22	26.61	5.15	0.07	32
FeSO ₄	31.48	38.13	7.91	0.07	15
Na ₂ S	21.67	28.62	6.00	0.06	26
NH ₄ HCO ₃	31.14	34.12	8.77	0.06	30
H ₂ SO ₄	32.50	43.25	7.36	0.07	21
C ₂ H ₂ O ₄	33.32	40.67	4.50	0.06	23
Water Glass, CuSO ₄	28.77	72.41	8.21	0.06	17
Water Glass, FeSO ₄	27.08	70.62	6.39	0.07	18
Water Glass, Na ₂ S	27.27	65.50	6.24	0.06	21
Water Glass, NH ₄ HCO ₃	26.81	72.87	5.94	0.07	13
Water Glass, H ₂ SO ₄	28.81	68.51	5.78	0.07	20
Water Glass, C ₂ H ₂ O ₄	29.20	73.62	7.53	0.07	15
Water Glass, C ₂ H ₂ O ₄ +FeSO ₄	27.30	77.45	7.13	0.07	18
Water Glass, C ₂ H ₂ O ₄ +NH ₄ HCO ₃	28.86	73.82	6.33	0.07	14
Water Glass, H ₂ SO ₄ +CuSO ₄	28.85	64.38	8.67	0.07	12
Water Glass, FeSO ₄ +NH ₄ HCO ₃	30.63	61.67	7.25	0.07	15

performance of the pulp, which, in turn, improves its recovery. On the other hand, when the FE value in each activation process reaches the maximum, the flotation index is not the best, indicating that the generated foam volume is not the larger the more beneficial. The FC value of other activated processes is generally 0.06 or 0.07, which is higher than the 0.05 of the unactivated flotation process. It shows that the flotation recovery may be improved by adding reagents to improve the foaming performance when the aeration volume is fixed. However, as the recovery increases, the grade will decrease. The majority of the FSI of dispersion-activation flotation and dispersion-combined activation flotation with superior flotation indexes are less than 20 s, and nearly all of the FSI of unactivated flotation and conventional activation flotation with inferior flotation indexes are greater than 20 s. It can be indicated that a reduction in foam stability may facilitate enhanced recovery for floatability.

4. Conclusions

All the activation flotation processes can help to improve the frothing performance of the slurry, which in turn improves the flotation recovery. Dispersion-activation flotation and dispersion-combined activation flotation can reduce the FSI to less than 20 s, which can help to improve the recovery of the raw ore flotation by reducing the stability of the froth; for the activated flotation processes to achieve the optimal flotation indexes, the frothing performance and froth stability of the slurry are close to each other. The foam stability is close to each other. This shows that the activation in different ways can improve the flotation indexes by changing both the frothing performance of the slurry and the stability of the generated foam. The optimal reagent combination was water glass + $C_2H_2O_4$ + $FeSO_4$. The results of this study show that the activator can also affect the nature of the flotation froth, which in turn affects the flotation indexes.

Acknowledgments

The project was supported by the National Natural Science Foundation of China (52004069).

References

- AI MAHROUQI, D., VINOGRADOV, J., JACKSON, M.D., 2017. *Zeta potential of artificial and natural calcite in aqueous solution*. *Adv. Colloid Interfac.* 240, 60-76.
- BAI, S., BI, Y., LI, J., YU, P., DING, Z., LV, C., WEN, S., 2021. *Innovative utilization of acid mine drainage (AMD): A promising activator for pyrite flotation once depressed in a high alkali solution (HAS)–Gearing towards a cleaner production concept of copper sulfide ore*. *Miner. Eng.* 170, 106997.
- CAN, İ.B., ÖZÇELİK, S., EKMEKÇI, Z., 2021. *Effects of pyrite texture on flotation performance of copper sulfide ores*. *Minerals.* 11(11), 1218.
- CHEN, H., CHEN, Z., WEI, B., JIANG, Q., 2023. *A novel approach for quantitative characterization of aqueous in-situ foam dynamic structure based on fractal theory*. *Fuel.* 352, 129149.
- CLAREMBOUX, V., 2020. *Role of flocculation and dispersion in pelletization of iron ore*. (Master's thesis, Michigan Technological University).
- DENG, J., LIU, C., YANG, S., LI, H., LIU, Y., 2019. *Flotation separation of barite from calcite using acidified water glass as the depressant*. *Colloid. Surface. A.* 579, 123605.
- FU, Y., HOU, Y., WANG, R., WANG, Y., YANG, X., DONG, Z., LIU, J., MAN, X., YIN, W., YANG, B., TANG, H., 2021. *Detailed insights into improved chlorite removal during hematite reverse flotation by sodium alginate*. *Miner. Eng.* 173, 107191.
- GAVRILLOVA, T.G., KONDRAT'EV, S.A., 2020. *Effect of physisorption of collector on activation of flotation of sphalerite*. *J. Min Sci.* 56(3), 445-456.
- JEFFERSON, M., YENIAL-ARSLAN, U., EVANS, C., CURTIS-MORAR, C., O'DONNELL, R., PARBHAKAR-FOX, A., FORBES, E., 2023. *Effect of pyrite textures and composition on flotation performance: A review*. *Miner. Eng.* 201, 108234.
- JIANG, K. HAN, Y., LIU, J., WANG, Y., GE, W., ZHANG, D., 2023. *Experimental and theoretical study of the effect of pH level on the surface properties and floatability of pyrite*. *Appl. Surf. Sci.* 615, 156350.

- JOHN, J., EVANS, C., JOHNSON, N.W., 2020. *The influence of lime and sodium hydroxide conditioning on sulfide sulfur behaviour in pyrite flotation*. Miner. Eng. 151, 106304.
- KOVALCHUK, E.V., TAGIROV, B.R., BORISOVSKY, S.E., NICKOLSKY, M.S., TYUKOVA, E.E., SIDOROVA, N.V., KOMAROV, V.B., MEZHUEVA, A.A., PROKOFIEV, V.Y., VIKENTYEV, I.V., 2024. *Gold and arsenic in pyrite and marcasite: Hydrothermal experiment and implications to natural ore-stage sulfides*. Minerals. 14, 170.
- LI, Z., HANAOKA, T., 2020. *Development of large-point source emission downscale model by estimating the future capacity distribution of the Chinese iron and steel industry up to 2050*. Resour. Conserv. Recy. 161, 104853.
- LIU, S., GE, Y., FANG, J., YU, J., GAO, Q., 2020. *An investigation of froth stability in reverse flotation of collophane*. Miner. Eng. 155, 106446.
- MASOTTA, M., ROCCHI, I., PAZZAGLI, G., D'AMBROSIO, R., SEGGIANI, M., 2021. *Recovery of sulfur from sulfur-rich filter cakes in a rotary kiln: Process optimization*. Waste. Manage. 126, 567-577.
- MORENO, Y.S., BOURNIVAL, G., ATA, S., 2021. *Foam stability of flotation frothers under dynamic and static conditions*. Sep. Purif. Technol. 274, 117822.
- NAYAK, A., JENA, M.S., MANDRE, N. R., 2022. *Beneficiation of lead-zinc ores—a review*. Miner. Process. Extr. M. 43(5), 564-583.
- NLEYA, Y., SIATE, G.S., NDLOVU, S., 2016. *Sustainability assessment of the recovery and utilization of acid from acid mine drainage*. J. Clean. Prod. 113, 17-27.
- NYSTRÖM, E., KAASALAINEN, H., ALAKANGAS, L., 2019. *Prevention of sulfide oxidation in waste rock by the addition of lime kiln dust*. Environ. Sci. Pollut. R. 26, 25945-25957.
- QUEZADA, G.R., PICEROS, E., ROBLES, P., MORAGA, C., GÁLVEZ, E., NIETO, S., JELDRES, R.I., 2021. *Polyacrylic acid to improve flotation tailings management: Understanding the chemical interactions through molecular dynamics*. Metals. 11(6), 987.
- TANER, H.A., ONEN, V., 2024. *Mechanism of mechanical entrainment in chalcopyrite flotation: Effects of clay minerals*. Mining. Metall. Explor. 41(1), 311-319.
- WANG, Q., WANG, D., SHEN, Y., WANG, H., XU, C., 2017. *Influence of polymers on dust-related foam properties of sodium dodecyl benzene sulfonate with Foamscan*. J. Disper. Sci. Technol. 38(12), 1726-1731.
- WANG, J., CAO, Y., LI, G., DENG, L., LI, S., 2018. *Effect of CTAB concentration on foam properties and discussion based on liquid content and bubble size in the foam*. Int. J. Oil. Gas. Coal. T. 6(1), 18-24.
- WANG, L., WANG, G., GE, P., SUN, W., TANG, H., HU, W., 2022. *Activation mechanisms of quartz flotation with calcium ions and cationic/anionic mixed collectors under alkaline conditions*. Colloid. Surface. A. 632, 127771.
- WANG, L., WEI, B., WANG, H., SHEN, P., LIU, D., 2024. *Effect of lead ions treatment on the flotation behavior of lime-depressed pyrite in a butyl xanthate system*. Sep. Purif. Technol. 128398.
- WENG, W., ZHANG, W., LIN, H., CHI, X., ZHONG, S., 2023. *Fixing sulfur dioxide by feeding calcine oxide into the rotary volatilization kiln in the zinc smelting plant*. Environ. Sci. Pollut. R. 30.1, 43768-43777.
- YANG, W., FENG, Q., HAN, G., 2023. *A novel activation approach for promoting chrysocolla flotation: Performance and mechanism*. Appl. Surf. Sci. 640, 158426.
- ZHANG, Q., WEN, S., FENG, Q., LIU, Y., 2021. *Activation mechanism of lead ions in the flotation of sulfidized azurite with xanthate as collector*. Miner. Eng. 163, 106809.
- ZHANG, Y., CHEN, H., CHENG, J., TIAN, J., ZHANG, L., OLIN, P., 2022. *Pyrite geochemistry and its implications on Au-Cu skarn metallogeny: An example from the Jiguanzui deposit, Eastern China*. Am Mineral. 107.10, 1910-1925.
- ZHAO, F., YU, X., GAO, X., LI, M., CHEN, X., 2023. *The selective depression effect of sodium hexametaphosphate on the separation of chlorite and specularite*. Physicochem. Probl. Mi. 59.
- ZHOU, H.P., HU, J., ZHANG, Y.B., CAO, Y.J., LUO, X.P., TANG, X.K., 2020. *Effectively enhancing recovery of fine spodumene via aggregation flotation*. Rare Metals. 39, 316-326.